We are IntechOpen, the world's leading publisher of Open Access books Built by scientists, for scientists

6,900
Open access books available

186,000
International authors and editors

200M
Downloads

Our authors are among the

154
Countries delivered to

TOP 1%
most cited scientists

12.2%
Contributors from top 500 universities

CLARIVATE ANALYTICS
BOOK CITATION INDEX
INDEXED

WEB OF SCIENCE™

Selection of our books indexed in the Book Citation Index
in Web of Science™ Core Collection (BKCI)

Interested in publishing with us?
Contact book.department@intechopen.com

Numbers displayed above are based on latest data collected.
For more information visit www.intechopen.com

Chapter

Reliable Positioning and Journey Planning for Intelligent Transport Systems

Ahmed El-Mowafy, Nobuaki Kubo and Allison Kealy

Abstract

Safety and reliability of intelligent transport systems applications require positioning accuracy at the sub-meter level with availability and integrity above 99%. At present, no single positioning sensor can meet these requirements in particular in the urban environment. Possible sensors that can be used for this task are first reviewed. Next, a suggested integrated system of low-cost real-time kinematic (RTK) GNSS, inertial measurement units (IMU) and vehicle odometer is discussed. To ensure positioning integrity, a method for fault detection in GNSS observations and computation of the protection levels (PL) that bound the position errors at a pre-set risk probability of the integrated sensors are presented. A case study is performed for demonstration. Moreover, to save energy, reduce pollution, and to improve the economy of the trip, proper journey planning is required. A new approach is introduced using 3D city models to predict the route with the best positioning integrity, availability and precision for route selection among different possible routes. The practical demonstration shows that effectiveness of this method. Finally, the potential of using the next generation SBAS for ITS applications was tested using kinematic tests carried out in various environments characterized by different levels of sky-visibility that may affect observations from GNSS.

Keywords: intelligent transport systems, positioning, GNSS, IMU, odometer, integrity monitoring, SBAS, prediction

1. Introduction

Intelligent transport systems (ITS) require reliable, continuous, accurate and cost-effective vehicle positioning in real time and in different weather and work conditions with for lane identification and control of vehicles. Normally, the width of the lane is about 2.8–3.5 m and that of the car is about 2 m. Therefore, better than 1 m horizontal accuracy is required to recognize the lane and 0.1 m horizontal accuracy is needed to control the vehicle [1]. The work environment of ITS is also very dynamic, changing between open sky, semi-urban to urban where vehicles may be surrounded by other vehicles and travel in overpass, tunnels, etc. In such dynamic environment, and due to limitations in the capabilities, and performance of available positioning sensors, such as global navigation satellite systems (GNSS), inertial measuring units (IMU), odometers, cameras and radar, it is hard to depend solely on one system, but rather on integrated set of sensors. For example, some ITS

applications rely on light detection and ranging with the help of cameras and radar. However, cameras sometimes cannot recognize the lane since the white line sometimes disappeared, and cameras are less reliable during foggy weather and at night. Similarly, while GNSS provides a primary positioning system, its signals can easily be obstructed in the urban environment. Thus, GNSS needs to be integrated with other sensors such as inertial measurement units (IMUs) to bridge positioning during GNSS positioning outages [2, 3]. To help the on-board positioning systems, methods such as cooperative positioning were proposed [4]. When selecting sensors, one should note that their cost varies much according to their quality; yet, the car industry can only afford a combination of sensors with a total cost that does not exceed a few hundreds of dollars. Therefore, low cost sensors, which may have limited capabilities, are used.

For ITS safety applications, not only accuracy is needed, but also integrity and reliability. Positioning integrity is a key performance parameter, where the system should be able to detect and exclude measurement faults, bound measurement errors, and trigger an alarm in the event that unreliable positioning performance is suspected. In addition, when no fault is detected, a protection level (PL) should be computed to bound the true position error at a certain probability of risk [5]. Integrity monitoring (IM) is currently being applied in aviation using an advanced receiver autonomous integrity monitoring (ARAIM) approach, which relies on the use of multi-frequency and multi-constellation phase-smoothed pseudo-range observations [6–8]. However, limited research has been done for applications such as ITS which require precise positioning that utilizes carrier-phase observations. Some examples are given in [9] when positioning using relative positioning, in [10] using precise point positioning (PPP) method, and in [11] using Real-Time Kinematic (RTK) method. At the moment, integrity requirements in vehicular transport have not been defined yet, but the demand for higher levels of automation in an increasing number of applications is pushing the relevant authorities to urgently fill this gap.

Up to now, most IM proposed methods focused on applying ARAIM in aviation and only employing GNSS measurements. Such integrity monitoring for transport applications has been addressed in a few studies, for instance in [12–14], where the focus was primarily on the use of single-frequency code observations. However, for ITS, GNSS cannot be used solely, and hence new IM methods are needed when integrating GNSS with other sensors [15]. In this article, the PLs that bound the position error are presented for continuous positioning of vehicular applications by integrating, in a simple fusion, loosely coupled algorithm low-cost RTK GNSS using code and phase observations supplemented by Doppler measurements, combined with low-cost IMU and vehicle odometer data. For GNSS we restrict our focus to horizontal positioning for the along-track and cross-track positioning of the vehicles, which are of interest for lane identification and collision warning.

For journey planning, to ensure reliability, and to save energy and reduce trip time, prediction of GNSS positioning integrity and precision are presented using 3D city models [16, 17]. The 3D city model also helps in identifying non-line of sight (NLOS) GNSS signals, which is a source of error. In addition, while RTK or network RTK [18] requires data from reference stations, the use of satellite based augmentation systems (SBAS) [19], does not have this requirement where sub-m accuracy in a stand-alone mode can be obtained. Therefore, results from testing the new generation of SBAS of the Australian test bed applied for ITS in various work environments are presented. This SBAS comprises the traditional L1 legacy SBAS signals for GPS only, the new dual-frequency multi-constellation (DFMC) SBAS and SBAS-based PPP using measurements from GPS and Galileo measurements. The following sections describe these methods, and their performance is demonstrated through tests representing ITS applications.

2. Positioning in ITS

2.1 GNSS and IMU as the main positioning sensors

There is a range of GNSS methods that can be used for transportation applications. Their features and accuracy are summarized in **Table 1**. The single point positioning (SPP) and Differential GPS (DGPS) use only one receiver, and employ single-frequency undifferenced code observations for the former and with corrections of satellite-related errors (satellite orbit and clocks corrections) in the latter, making them affordable and widely used for vehicle navigation. However, both approaches provide several meters of positioning error, and thus they are not suitable for ITS. With the sub-m requirement of ITS, only three methods can be used, namely real-time kinematic (RTK) [20] or network RTK (NRTK) [18], precise point positioning (PPP) [21, 22], and the next generation SBAS [19]. The advent of low-cost dual-frequency multi-constellation GNSS, at the level of a few hundreds of dollars, allow their use in advanced vehicle positioning. Their performance has recently been remarkably improved, at a few cm accuracy.

For the IMU (also known as inertial navigation system (INS), typically after obtaining a navigation solution), the strategic grade type provides the best performance, but at a high cost and thus is not suitable for vehicle applications. However, small, robust, and low-cost inertial sensors, e.g. the micro electrical mechanical sensors (MEMS) IMUs [23], have been available in the market for several years, which can be used in vehicle navigation. They, however, suffer from the rapid growth of their biases. The solutions obtained from GNSS and IMU complement each other, as they have different characteristics, summarized in **Table 2**. GPS solution aid IMU by resetting the accumulation of its bias. On the other hand, IMU can extrapolate solutions at a higher rate and can cover positioning during short GNSS outages. IMU additionally provides the attitude (orientation) that can also be

Features	SPP	DGPS	SBAS	RTK (Sing Ref. and NRTK)	PPP
No. of receivers	one	one	one	2 (RTK) 1 (NRTK)	one
No. of Observation Frequencies	one (e.g. L1)	one (e.g. L1)	one (e.g. L1) 2 DFMC (L1&L5)	2 (e.g. L1&L2 or L1&L5)	2 (e.g. L1&L2 or L1&L5)
Need for data or corrections	Autonomous	Reference station corrections	Orbit + clock corr. (+iono for L1)	Reference station data	Orbit + clock corrections
Main observations	Code obs.	Code obs.	Code obs.	Code + phase obs.	Code + phase obs.
Accuracy	1–6 m	Sub-m to a few-m	Sub-m to 1.5 m	Few cm	Dm (float), cms (fixed)
Solution type	Snap shot	Snap shot	Snap shot	Kalman or sequential LS	Kalman filter or seq. LS
Main issues	Low accuracy - noisy	Low accuracy - noisy	Not suitable for urban	Ambiguity fixing	Long time for Convergence
Suitable for ITS	No	No	In open sky only	Yes	Yes

Table 1.
Features of GNSS methods used for positioning in transportation.

used in estimating the positioning errors along the vehicle direction of motion, which is needed for a more representative integrity monitoring as will be explained later, and in applications such as collision alert.

2.2 Simple integration of low-cost GNSS, IMU and odometer

In this article, low-cost systems that are suitable for vehicle applications are considered. Two approaches can be applied to control the growth of heading bias of the MEMS IMU. At the start, or when the vehicle stops, e.g. at red traffic lights, the zero velocity update (ZUPT) is applied. When GNSS data is available, it is used to reset the heading bias of the MEMS IMU. The GNSS position and velocity are coupled with the IMU output using Kalman Filter in loosely- or tightly-coupled schemes. While the tightly coupled integration is beneficial in the case when GNSS cannot estimate the position, e.g. due to a low number of visible satellites, the IMU data can be used to slightly predict the pseudo-range observations; however, it is impossible to predict the carrier phase observations at the level of ambiguity fixed solution. Therefore, for the low-cost RTK/IMU systems, no practical difference exists between using loosely and tightly coupled integration.

In RTK a minimum of five satellites should be observed. When observing four satellites, e.g. in a semi-urban environment, a simple approach can be applied for positioning using the low cost systems. GNSS Doppler velocities can be used to compute initial values of IMU heading and to calibrate it at short intervals to control the growth of its bias [24]. The computed heading from Doppler measurements at time t (denoted as θ_t) is calculated from the average $\theta_t = tan^{-1}\left(\frac{V_{E_t}}{V_{N_t}}\right)$, where V_{E_t} and V_{N_t} are the Doppler-based velocity components in the local-level frame. Thus, the accuracy of heading obtained from GNSS depends on the velocity measurements and partly on the dilution of precision (DOP), which is an indicator of the number and geometry of observed satellites (their distribution in the sky). When the speed of the vehicle is low, the heading from GNSS is not reliable because the computed GNSS velocity would be noisy in the order of a few centimeters per second. In addition, the sampling rate of GNSS is less than that of the heading rate of the MEMS IMU; therefore, when the road suddenly bends, the obtained heading could deviate several degrees from the actual orientation of the vehicle. Consequently, several conditions were set to use GNSS for calibrating the IMU heading error to below two degrees. These conditions include VSS > 0.5 m/s; $|V_{GNSS} - V_{SS}|$ < 0.5 m/s; VSS > 0.5 m/s, where V_{GNSS} and V_{ss} are the velocities estimated by the GNSS and vehicle's odometer, respectively. Large errors of the heading obtained from the GNSS should not be used. Therefore, the heading from the GNSS must

GNSS	IMU
Absolute positioning	Relative positioning
Good accuracy in long term	Good accuracy in short term
Attitude available—need multiple units	Attitude available—single unit
Low sampling rate (1–10 Hz)	High sampling rate (e.g. 100 Hz)
Subject to signal blockage	Not related to surrounding environment
Low-cost can provide good accuracy	Low-cost provides poor accuracy
Biases are stable	Biases grow with time

Table 2.
Characteristics of GNSS and IMU.

always be checked, with a threshold in the order of 2°, using both the best estimated heading in the previous epoch and the heading rate of the IMU, as the heading rate obtained from the IMU in a short period is accurate.

If RTK is unavailable, the positions can be estimated by integrating the speed estimated from the vehicle odometer with the heading of the MEMS IMU. The time increments of position components in North and East (ΔE, ΔN) is computed, such that $\Delta E = V_{ss} \times \sin(\theta) \times \Delta t$ and $\Delta N = V_{ss} \times \cos(\theta) \times \Delta t$, where θ is the heading estimated by the IMU and Δt is the time increment. The velocity and azimuth considered are the mean values during the time increment. The odometer equipped in the vehicle is used to obtain the distance information of the car. Normally, a velocity pulse generation device counts the number of pulses per rotation of the wheel. In this study, we use the speed pulse obtained from the POSLVX system, which is a wheel-mounted rotary shaft encoder that accurately measures the linear distance covered by the vehicle [25]. The two methods, Doppler calibrated IMU and Odometer+IMU, can only estimate temporal position changes, and hence, their positioning errors accumulate with time, in particular, the heading bias of the IMU. Therefore, they should only be restricted to bridging short breaks in RTK as will be discussed later by an example.

2.3 SBAS for ITS

The positioning accuracy of the traditional SPP method can be improved by using orbital and clock corrections from the satellite based augmentation systems (SBAS). SBAS can provide meter-level accuracy in a stand-alone mode without the need for relative positioning with a nearby base station that is required in RTK. However, traditional SBAS systems, such as the United States WAAS system or the European EGNOS system augment only L1 single frequency measurements. Therefore, the ionosphere delays need to be processed and delivered to the users. This makes single-frequency SBAS sensitive to the distribution of the ground network used to compute the ionosphere corrections, have a limited coverage area, and are less precise during rapid fluctuations of the ionosphere.

The second-generation SBAS, such as that implemented in the under-development Australia SBAS, includes in addition to the traditional L1 legacy SBAS signals, dual-frequency multi-constellation (DFMC) SBAS signals that are transmitted over L5 for GPS L1/L5 and Galileo E1/E5a signals. Hence, the user can apply ionosphere-free combination without the need for ionosphere corrections. This allows the user to work anywhere within the footprint of the SBAS satellite and is not sensitive to ionosphere fluctuations. Moreover, the second generation SBAS includes precise orbits and satellite clock corrections to enable precise point positioning (PPP) service with float-ambiguity solution type. This can provide dm level accuracy, which is suitable for ITS. Furthermore, the multi-constellation scenario will increase the number of satellites and thus provides users with a better measurement geometry. Results from testing the new generation of SBAS when applied for ITS in various work environments are presented in the testing section.

2.4 Cooperative positioning

The recent developments in vehicular ad-hoc networks (VANETs) and dedicated short range communication (DSRC) support the principle of cooperative positioning (CP) through wireless connectivity. CP has been proposed to share positioning information obtained from each individual vehicle, connected to the system, to increase the vehicle awareness of the surrounding vehicles, predict potential incidents, threats, and hazards on the road with an increased time horizon

and awareness distance that is beyond what in-vehicle technologies (radars or cameras) and the driver can visualize [26].

In the vehicle-to-vehicle (V2V) and vehicle-to-infrastructure (V2I) communications, vehicles send messages to each other or to infrastructure. These messages include their temporary ID, location, speed, heading, lateral and longitudinal acceleration, brake system status, and vehicle size [27]. Sharing this data in the V2V communication can provide warnings to the drivers in poor vision scenarios during the rear end or intersection collision and lane change. Examples of V2I benefits include awareness of unsafe conditions on the road, including fog, ice, and Eco-approach and departure at signalized intersections.

The positions of all nodes in the in the VANET network can be determined by integrating this information in either a centralized or decentralized algorithm. An alternative concept relies either on the availability of ranging information to other vehicles using V2V communication or the availability of ranging information to DSRC roadside units (RSUs) using V2I [28]. Other CP methods leverage the communications signal as a ranging signal. For instance, methods such as signal strength-based ranging, time-based ranging including time of arrival (TOA) and time difference of arrival (TDOA) methods have been implemented however, these produce errors at several meters, which makes them not suitable for ITS. On the other hand, Non Ranging-Based techniques do not rely on time or signal strength ranging techniques, and thus, have fewer errors, but they are expensive since it requires RSUs, installed at each intersection, storing information about the road geometry. Several approaches were proposed to enable CP in the framework of VANET, while each method has merit, it has also limitations. This idea of ranging between nodes in the network has led to sensors such as ultra wide band and radar being deployed as part of the multi-sensor suite to overcome some of the limitations associated with ranging from DSRC signals.

Based on this discussion of CP, as depicted in **Figure 1**, two distinct subsets of navigation systems are used to define a CP architecture. The first is termed as local level, where each vehicle takes its own measurements and would be able to provide its own position estimate, independent of other vehicles. This system typically consists of GNSS and IMU. The second is termed as network level, where vehicles would share information among each other to form a network, using DSRC and UWB, to provide a more robust position estimate in GNSS denied environments. The advantages of the network approach over the local level are: the additional inter-vehicle measurements provide greater measurement redundancy and consequently improve the precision and robustness of the solution. In sharing measurements, vehicles with insufficient measurements to determine a local level solution, are still able to determine their position, thereby improving the availability of positioning solutions across the whole network. A network approach is also scalable to a large number of nodes,
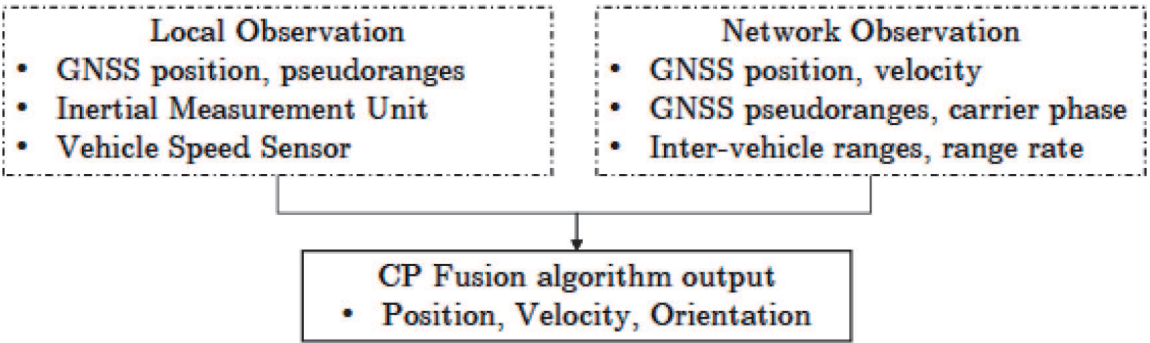

Figure 1.
Local and network level observations.

using a decentralized processing approach, a large network can share information in a way that maintains the optimal estimate for each node, whilst balancing the computational overheads. This allows this approach more computationally efficient compared to centralized processing at each node in the local level.

3. Route selection

For ITS, reliable real-time positioning should be maintained all the time. In addition, for the driver convenience and to save energy and reduce pollution by reducing journey time and improving the economy of a trip, proper journey planning is required by the computer on board the ITS vehicle before the start of the Journey. The route with best positioning performance in terms of integrity availability and precision, in addition to other parameters such as trip time and distance, is selected among different possible routes. Prediction of these parameters can be best performed using 3D city models when using GNSS, where a minimum of five satellites need to be observed to enable GNSS-RTK positioning. The method is also suitable to determine locations within the city, at different times of the day that GNSS would not be suitable and other sensors should be used.

The general procedure to predict the satellites that are in view and the existence of LOS (LINE-OF-SIGHT) between a GNSS satellite and GNSS receiver using a 3D city model for each location along candidate routes comprises the following four steps:

a. *Identify the receiver position*: The vehicle position is first approximately estimated at each epoch according to time and location of the start of the journey, speed of the vehicle (taken as the road speed), and the centerline of the lane that has the worst satellite geometry, typically the nearest to the nearby buildings. A change of position of ~20 m/s is expected, therefore, the LOS checking should be performed at short time intervals, e.g. 2–10 Hz.

b. *Estimate satellite positions*: The satellite positions are predicted using satellite navigation file, according to the expected time of processing. Due to the slow change of satellite geometry, an actual delay or advance of a few minutes between the actual and prediction time would not make a significant difference in the satellite geometry, and hence in the prediction result.

c. *Establishment of buildings and terrain data*: The location, size, height and orientation of each building along the route are constructed from 3D polygon data. Buildings and terrain data are prepared separately and later are combined. **Figure 2** shows an example of 3D models that were created for our research. More details will be given in the testing section.

d. *Assessing the existence of LOS between satellites and the receiver*: The presence of LOS between possible satellites in view from the almanac and the receiver can be determined by checking whether the direct line connecting the satellite and the receiver intersects with the building. By modeling the building as triangular meshes, it is possible to determine the presence of an intersection as shown in **Figure 3** using the following method presented in [29]. In this figure, S indicates the satellite position and R represents the receiver's location. B_1, B_2 and B_3 are the vertices of a triangular face of the building meshed surface facing the receiver. Let s, r, b_1, b_2 and b_3 be the corresponding position vectors in an arbitrary reference frame, and u_{ij} be the unit vector from B_i to B_j. Likewise, let point P be the intersection between the vector
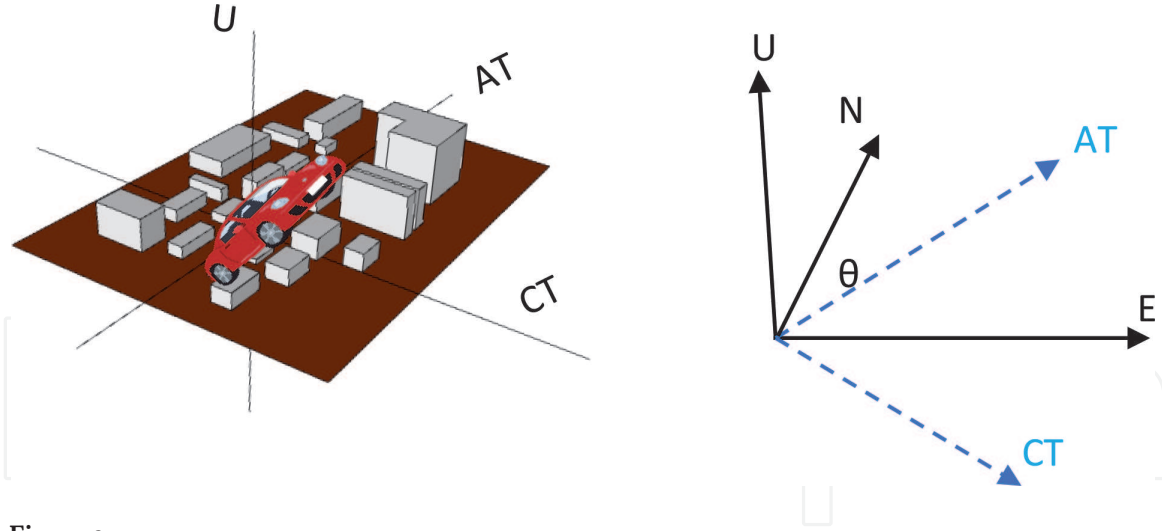
Figure 2.
Example of buildings and terrain data of 3D city model (left), showing the AT-CT and N-E (right). θ is the azimuth.
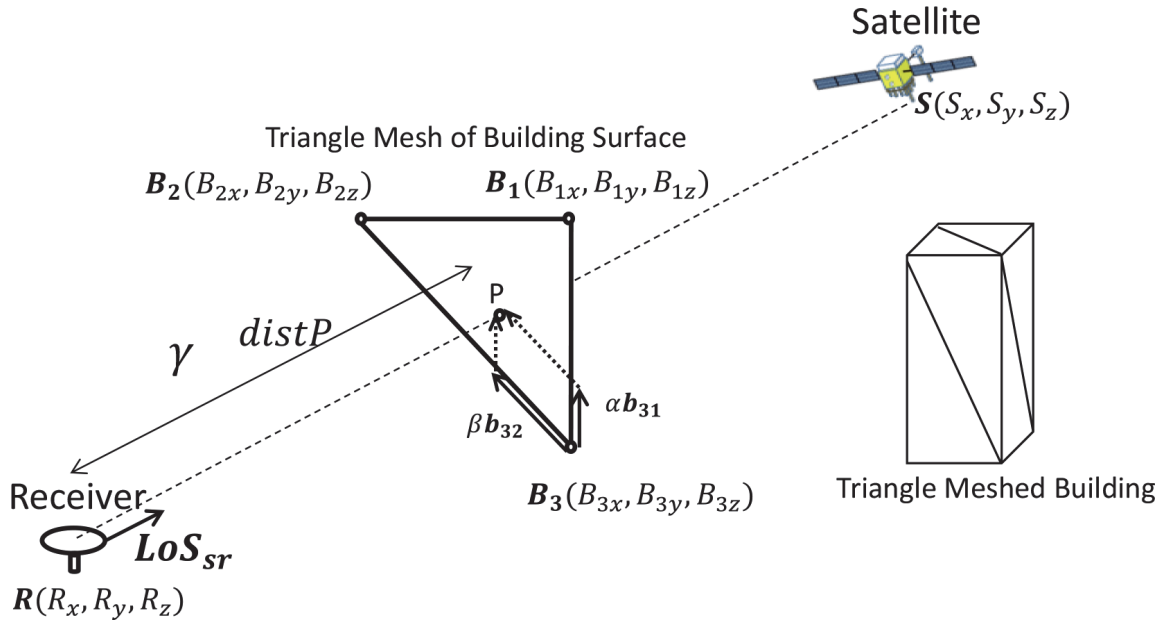

Figure 3.
Prediction of the satellite LOS.

between the receiver and the satellite, which unit direction vector is indicated by u_{LOS}, and the triangular mesh, and p is the corresponding position vector. In the vector space we have:

$$p = r + \gamma\, u_{LOS} \text{ and } p = b_1 + \alpha\, u_{13} + \beta\, u_{12} \qquad (1)$$

where γ is the distance between R and P. α and β are the coordinates of P in a local frame that includes the sides of the mesh triangle as principle axes. The system in (1) can be solved for γ, α, and β. Thus, the conditions for P to be included in the triangular mesh, and therefore No LOS (NLOS) are:

$$\gamma \geq 0; 1 \geq \frac{\alpha}{|b_1 - b_3|} \geq 0;$$

$$1 \geq \frac{\beta}{|b_1 - b_2|} \geq 0; 1 \geq \frac{\alpha}{|b_1 - b_3|} + \frac{\beta}{|b_1 - b_2|} \geq 0 \qquad (2)$$

Otherwise, the satellite position is considered in LOS. The geometry of the visible satellites is then examined to check sufficient positioning precision can be obtained, and check integrity as will be discussed in the next section.

4. Integrity monitoring

Integrity monitoring includes the ability of the system to detect and exclude faulty observations (known as FDE) and to alarm the user if a protection level (PL) that bounds the true position error at a specific risk probability is less than an alarm limit (AL). Integrity monitoring is considered available when PL < AL. Both tasks, i.e. FDE and computation of PL, are addressed in the following sub-sections.

4.1 Fault detection

In general, the equation of the fault-free observations can be expressed as:

$$y = G\,x + \varepsilon \tag{3}$$

where y is the measurement vector, computed as the difference between the observations and their estimated values from the approximate user and satellite positions. The null hypothesis is expressed as H_0: E{y} = $G\,x$ with D{y} = Q_y, representing the covariance matrix of the observations, where E{} and D{} denote the expectation and dispersion operators, respectively. The unknown vector x is the difference between the final and the approximate vehicle's computed positions. ε is the observation error, assumed noise in the fault-free case with zero mean and Gaussian distribution. The G matrix for RTK is the direction cosine matrix.

For the IMU + odometer, the observations are the Easting and Northing velocity components computed as $V_E = V_{ss} \times \sin(\theta)$, and $V_N = V_{ss} \times \cos(\theta)$. These velocities are integrated in time to provide the time changes in position in Easting and Northing directions. The observations are considered in this case as the mean values of the IMU heading (θ) and the odometer speed V_{ss}, for instance between the epochs $t\text{-}1$ and t. Thus, the G matrix is expressed as [25]:

$$G_t = \begin{bmatrix} \dfrac{\partial\,\theta}{\partial\Delta E} & \dfrac{\partial\,\theta}{\partial\Delta N} \\[2ex] \dfrac{\partial\,v}{\partial\Delta E} & \dfrac{\partial\,v}{\partial\Delta N} \end{bmatrix}_t = \begin{bmatrix} \dfrac{\Delta N}{\Delta E^2 + \Delta N^2} & \dfrac{-\Delta E}{\Delta E^2 + \Delta N^2} \\[2ex] \dfrac{\Delta E}{\Delta t \times \sqrt{\Delta E^2 + \Delta N^2}} & \dfrac{\Delta N}{\Delta t \times \sqrt{\Delta E^2 + \Delta N^2}} \end{bmatrix}_t \tag{4}$$

Using least squares for fault detection, the solution in (E-N-U) frame reads:

$$\hat{x} = R \left(G^T Q_y^{-1} G \right)^{-1} G^T Q_y^{-1}\, y = S\,y \tag{5}$$

where $S = R \left(G^T Q_y^{-1} G \right)^{-1} G^T Q_y^{-1}$ is the pseudo inverse, which maps the observations onto the unknowns. In RTK, R is the rotation matrix from the Cartesian frame, in which the GNSS satellite positions are expressed, to the E-N-U frame. When using IMU + odometer measurements, R is the identity matrix. To identify which observations are faulty, the solution separation method can be applied [6]. This is performed by computing a position solution unaffected by the fault, by excluding the suspected observations. An error bound around this solution is computed, and the difference between the position solution from all observations and

the fault tolerant position is accounted for. For each potential fault mode i, which may comprise one or more faulty observations, an analogous S_i matrix is computed by excluding the suspected observations, such that:

$$\hat{x}_i = S_i\, y \tag{6}$$

The discrepancy in the positional vector $|\hat{x} - \hat{x}_i|$ forms the base for checking the presence of observation faults, where in case of faulty measurements in mode i, the difference between the two solutions $\hat{x}$ and $\hat{x}_i$ will be significant. The standard deviations of this difference (σ_{dE_i}, σ_{dN_i}, σ_{dU_i}) are next computed as:

$$\sigma_q = \sqrt{a_k^T (S_i - S) Q_y (S_i - S)^T\, a_k} \tag{7}$$

k = 1, 2, 3 for dE_i, dN_i, dU_i, with $a_1^T = [1, 0, 0], a_2^T = [0, 1, 0]$, and $a_3^T = [0, 0, 1]$.

For ITS applications, where only horizontal positioning is considered, it is more convenient to conduct testing for the along-track (AT) and cross-track (CT) position directions [30, 12]. Assuming $\Delta \hat{x}_i = |\hat{x} - \hat{x}_i|$ has a zero-mean Gaussian distribution in the fault-free mode; and considering its components for the AT and CT directions, defined as $\Delta \hat{x}_{i_{AT}}$ and $\Delta \hat{x}_{i_{CT}}$. Then the normalized discrepancies, i.e. $\frac{|\Delta \hat{x}_{i_{AT}}|}{\sigma_{\Delta \hat{x}_{i_{AT}}}}$ and $\frac{|\Delta \hat{x}_{i_{CT}}|}{\sigma_{\Delta \hat{x}_{i_{CT}}}}$ will also have a zero-mean Gaussian distribution, and will be used as the test statistic, where $\sigma_{\Delta \hat{x} i_{AT}}$ and $\sigma_{\Delta \hat{x} i_{CT}}$ are the stds of $\Delta \hat{x}_{i_{AT}}$ and $\Delta \hat{x}_{i_{CT}}$ respectively. Therefore, when examining m possible fault modes, for i = 1 to m, setting a threshold of the standard normal distribution at a selected significance level, i.e. $N_{\frac{\alpha}{2 \times 2m}}(0, 1)$, a fault is suspected when:

$$H_{aiAT} : \frac{|\Delta \hat{x}_{iAT}|}{\sigma_{\Delta \hat{x}_{iAT}}} \geq N_{\frac{\alpha}{2 \times 2m}}(0, 1) \text{ and } H_{aiCT} : \frac{|\Delta \hat{x}_{iCT}|}{\sigma_{\Delta \hat{x}_{iCT}}} \geq N_{\frac{\alpha}{2 \times 2m}}(0, 1) \tag{8}$$

When the direction of the vehicle is not well defined, or when this direction rapidly changes, for instance during rapid turns, a conservative approach is to perform the FDE test in the direction of the maximum error. To this end, the maximum-minimum region defined along the semi-major and semi-minor axes of a horizontal confidence error ellipse can be tested. These directions are defined in the Eigen space by the orientation of the first and second Eigen vectors. The semi-major axis of the error ellipse, which represents the max std. $\sigma_{\Delta x_{imax}}$ equals $\sqrt{\xi 1_i}$, where $\xi 1_i$ is the first Eigenvalue. Similarly, the semi-minor axis of this error ellipse $\sigma_{\Delta x_{imin}}$ is calculated as $\sqrt{\xi 2_i}$, where $\xi 2_i$ represents the second Eigenvalue of $Q_{\Delta \hat{x}_i}$, the 2D variance matrix of $\Delta \hat{x}_i$ computed by applying the propagation law. Thus, the null hypothesis is rejected suspecting a fault in mode i when:

$$\frac{\left(\Delta \hat{x}_i^T \cdot \vec{E1}_i\right)^2}{\sigma_{\Delta x_{imax}}^2} + \frac{\left(\Delta \hat{x}_i^T \cdot \vec{E2}_i\right)^2}{\sigma_{\Delta x_{imin}}^2} \geq \chi_{\frac{\alpha}{m}}^2(df, 0) \tag{9}$$

where $\vec{E1}_i$ and $\vec{E2}_i$ denote the first and second Eigenvector of $Q_{\Delta \hat{x}_i}$.

4.2 Computation of the protection levels

In our work, the *PLs* are modeled on the basis of the multi-hypothesis solution-separation method [6]. In RTK, with $df > 0$, a position error bound is computed for each possible fault mode i that might be misdetected. The *PLs* can be computed by solving the equations [12, 30]:

$$2\,\psi\left(\frac{PL_{AT}-b_{oAT}}{\sigma_{\hat{x}oAT}}\right)+\sum_{i=1}^{N_a}P_i\psi\left(\frac{PL_{AT}-K_{fa}\sigma_{\Delta\hat{x}iAT}-b_{iAT}}{\sigma_{\hat{x}iAT}}\right)=\frac{1}{2}(P_{HMIH}) \qquad (10)$$

$$2\,\psi\left(\frac{PL_{cT}-b_{ocT}}{\sigma_{\hat{x}ocT}}\right)+\sum_{i=1}^{N_a}P_i\psi\left(\frac{PL_{cT}-K_{fa}\sigma_{\Delta\hat{x}icT}-b_{icT}}{\sigma_{\hat{x}icT}}\right)=\frac{1}{2}(P_{HMIH}) \qquad (11)$$

The components (b_{oAT} and b_{oCT}) and (b_{iAT} and b_{iCT}) are projected in the position space using S and S_i from b_o and b_i, which denote the sum of the maximum nominal biases in the observations under the fault-free and fault hypotheses, respectively. $\sigma_{\hat{x}oAT}$ and $\sigma_{\hat{x}iAT}$ are the stds for the AT position solution and $\sigma_{\hat{x}oCT}$ and $\sigma_{\hat{x}iCT}$ are for CT. Similarly, $\sigma_{\Delta\hat{x}iAT}$ and $\sigma_{\Delta\hat{x}icT}$ are the stds of $\Delta\hat{x}_{iAT}$ and $\Delta\hat{x}_{icT}$ respectively. The absolute value of the bias is considered to bound the worst case scenario and to ensure that the continuity requirement is met. $\psi(\ )$ is the tail probability of the cumulative distribution function of a Gaussian distribution. P_i is the a-priori probability of fault in the observations in the examined fault mode i, assuming the same probability for all observations from one system, which differ among systems. Since no standards are available yet for IM in ITS, P_{HMIH} of 10^{-5} is assumed. The K_{fa} becomes $\psi^{-1}\left(\frac{\alpha}{2m}\right)$, where we assume α = 1% in this article.

It is assumed here that the observation and the position errors follow a Gaussian distribution. In the open sky environment, this is valid, but in the urban environment, and due to multipath, the distribution could be biased and it could have multiple peaks. Additionally, in ITS and due to motion of the vehicle and the dynamic change of the nearby structures, causing multipath, multipath tends to randomize. One approach here is to deweight the observations that may experience large multipath, such that their contribution in the solution is minimized. Such multipath modeling is based on satellite elevation and azimuth, and the use of 3D city models to describe the geometry of the surrounding structures. Moreover, an overbounding Gaussian distribution with large stds [31] can be used. However, this would lead to large PLs, a loss in integrity availability. **Figure 4** shows a flowchart of the positioning and integrity monitoring process, which includes the FDE and computation of the PLs.

For the case of integrating the heading from MEMS IMU and speed estimated by the odometer, where df = 0, the PLs are expressed as:

$$PL_{AT,i}=K_{md,i}\sigma_{AT,i}+\sqrt{\left(\cos\theta a_1^T S\begin{bmatrix}b_{\theta_{IMU}}\\b_v\end{bmatrix}\right)^2+\left(\sin\theta a_2^T S\begin{bmatrix}b_{\theta_{IMU}}\\b_v\end{bmatrix}\right)^2}$$

$$PL_{CT,i}=K_{md,i}\sigma_{CT,i}+\sqrt{\left(\sin\theta a_1^T S\begin{bmatrix}b_{\theta_{IMU}}\\b_v\end{bmatrix}\right)^2+\left(\cos\theta a_2^T S\begin{bmatrix}b_{\theta_{IMU}}\\b_v\end{bmatrix}\right)^2} \qquad (12)$$

where $b_{\theta_{IMU}}$ is a scalar representing possible unaccounted for growth in IMU heading bias between the bias resetting, using, for instance, GNSS heading. It is assumed here that this bias increases linearly with time, such that $b_{\theta_{IMU}} = b_{\theta_o}+\Delta b\times\Delta t$, where b_{θ_o} is the initial bias, Δb is the bias drift with time, and Δt is the time difference between current epoch and the resetting epoch. b_v denotes the bias due to velocity measured by the odometer. $K_{md,i}$ is the inverse of the complement of the right-side standard normal cumulative distribution function (i.e. $K_{md,i}=\psi^{-1}(\beta)$) to satisfy the misdetection probability β, which can be preset. The final protection levels PL_{AT} and PL_{CT} are considered as the max$\{PL_{AT,i}\}$ and max$\{PL_{CT,i}\}$.
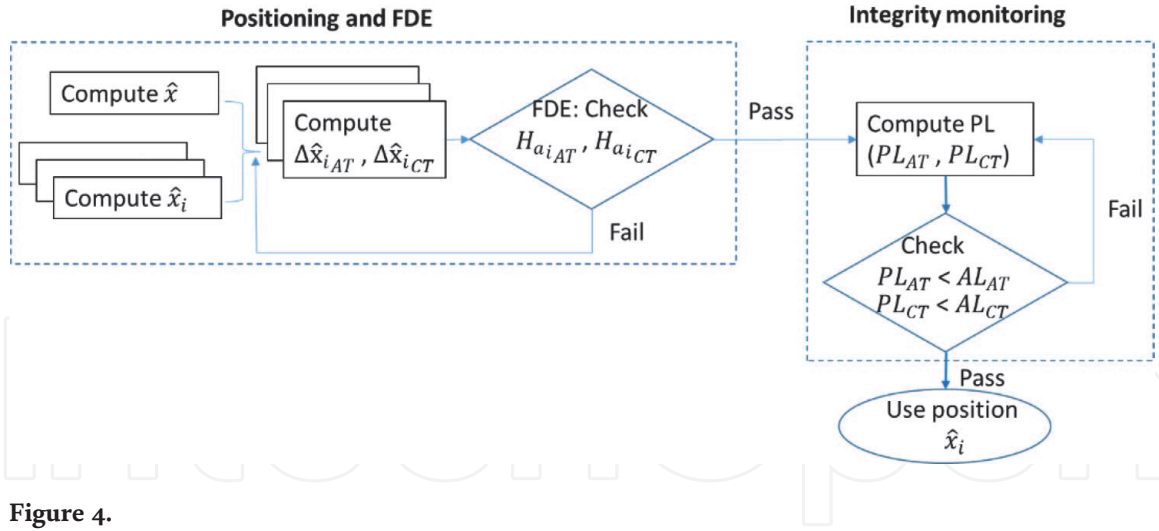
Figure 4.
Flowchart of the positioning, FDE and integrity monitoring process.

Since in the IMU + odometer case only time-changes of positions are measured, integrity risk has to additionally consider the accumulation of errors. The covariance matrix of the unknown coordinates (Q_{EN_t}) at time t can be expressed as:

$$Q_{EN_t} = G \, Q_{obs} G^T + Q_{EN_{t-1}} \qquad (13)$$

To bound the development of the accumulated error, this positioning approach needs to be reinitialized at short time intervals and the Q_{EN_k} is reset with each reinitialization. Such an approach will lead to a sawtooth-like pattern for the *PL* to adapt to the growth-reset error pattern.

5. Testing

In this section test results of an integrated GNSS/IMU/odometer system proposed for ITS are first presented and discussed. Afterwards, the next generation SBAS is tested when being implemented within an ITS setting.

5.1. Test description

A kinematic test was conducted using a small vehicle fitted with a low-cost RTK, MEMS IMU and odometer. The test is performed in semi-urban and urban environments in Tokyo, Japan. The road has 2–3 lanes on each side of the road, where several high-rise buildings were present. In addition, several overpasses, pedestrian bridges, and a river bridge were also present. The test trajectory is shown in **Figure 5**. The use of multi-system GNSS measurements is essential to observe enough number of satellites for RTK positioning and to resolve the ambiguities as quickly as possible to maintain reliability in this environment as the number of observed satellites changes frequently between 5 and 22. Therefore, the RTK system used GPS, GLONASS, QZSS and BeiDou dual-frequency observations with 10 Hz sampling interval. The RTK-GNSS was supported by Doppler frequency observations [32]. The Doppler-aided RTK-GNSS usually improves the fix rate by about 10–15% and provide the same reliability [33]. The positioning error (PE) in the RTK mode was estimated as the difference between the RTK-computed positions and those determined from post-mission kinematic processing (PPK) of the same data collected by the receiver but using independent software. The vehicle receiver operates within a few kilometers from a reference receiver occupying a known
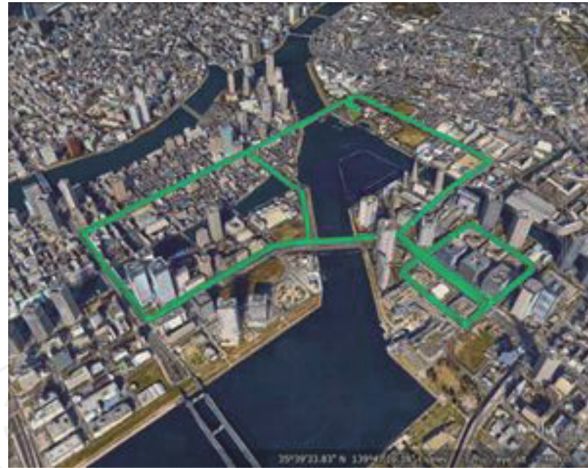
Figure 5.
Test trajectory in Tokyo.

point such that the spatially correlated errors; i.e. the broadcast orbital error and the atmospheric delays - ionosphere and troposphere, are canceled by double differencing the observations between the rover and the reference receiver, leading to ±5 cm accuracy [25].

A Bosch-consumer grade MEMS IMU was used in the test. The heading error of this IMU ranged from −2 to 5°, which can accumulate to 10° after 30 min without calibration [25, 34]. The raw 3-axis angular rate, 3-axis acceleration, and pressure are provided. The vertical position of the GNSS is integrated with the change in the vertical position deduced from the barometric sensor. If the velocity vector estimated by the GNSS is not available, the velocity vector estimated by the final integrated heading and speed sensor is used instead. If the absolute difference between these two velocity vectors is more than 0.25 m/s, we rely on the velocity vector estimated by the final integrated heading and odometer. The sampling rate of IMU and odometer was 100 Hz. For the odometer, the standard deviation of the computed speed is estimated as 5 cm/s, and for the speed determined from GNSS-Doppler measurements, it is 10 cm/s. The positioning errors when using IMU + odometer were computed by differencing their positions with the output from a POS/LV system (developed by Applanix Inc.), which was mounted on the vehicle and has a nominal positioning accuracy of approximately 20 cm.

The test was also used to demonstrate the performance of the prediction approach for selection of the best route based on best integrity availability and trip characteristics, such as distance and time of travel. Results of the predicted satellite positions and their geometry applying the 3D city model are compared with the real observed satellites obtained for the same route and the same period. The 3D city model is built using a GEOSPACE 3D solution numerical surface with polygon representation (http://www.ntt-geospace.co.jp/geospace/3d.html). The model includes land, roads, bridges, buildings, and vegetation. The 3D buildings are created by adding height information to the GEOSPACE digital 2D map, where the heights are measured from GEOSPACE aerial photographs (orthoimage). The accuracy of the models employed in this test is 2–3 m.

5.2. Route selection results

Figure 6(left) shows the difference between the number of satellites in view determined by the prediction algorithm and the number of the actually observed satellites along the test route. The difference in their satellite geometry, expressed by Position Dilution of Precision (PDOP), is illustrated in **Figure 6(right)**. The
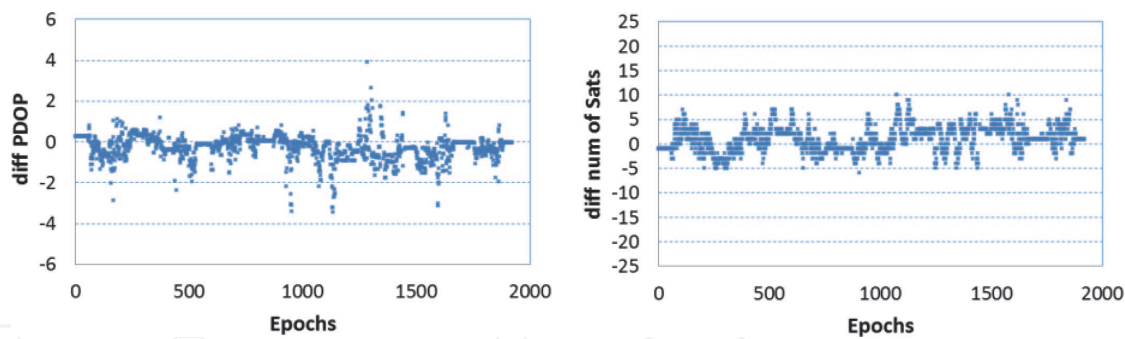
Figure 6.
Difference between using observed and predicted satellites in terms of: (left) number of satellites and (right) geometry expressed by PDOP.

results show that the average difference between the number of observed and predicted satellites in view is two satellites, ranging between ±5 satellites. The mean value of the absolute difference in PDOP is 0.461. Possible enhancement in this performance can be achieved by using more precise 3D models or maps. For instance, the 3D city models used here were of a medium accuracy of about 2–3 m in height estimation. More accurate 3D models at 1 m or better are available but at an extra cost. Better 3D maps can also be established from laser scanning, particularly in urban areas.

5.3. Accuracy and integrity monitoring results

Positioning in the above test was carried out using a system of combined RTK and IMU + odometer, where the latter method was required during gaps in RTK positioning spanning only short periods of up to 4 s, totaling about 3% of the entire test period. The position errors, computed as the difference between the solution from each of the positioning methods and the solution from a more precise system as explained in the previous section, are illustrated in **Figure 7**. **Table 3** shows the median of the absolute positioning errors and the RMSE for each mode. The median is used as it is less affected by outliers and skewed values of *PLs*. The table and **Figure 5** show that the RTK with correct ambiguity resolution provided positioning errors of a few cms and IMU + odometer provided sub-m level accuracy reaching 0.53 m after 4 s, which can grow to more than 2 m in less than 20s if left without
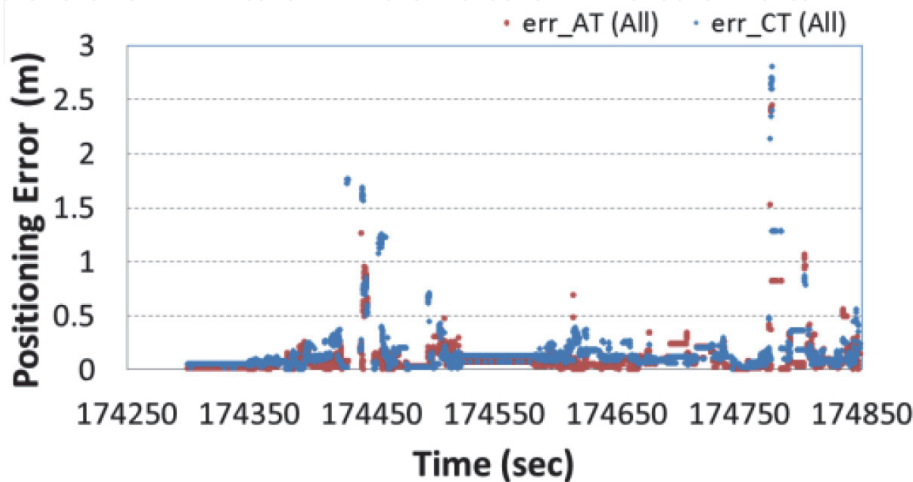

Figure 7.
Difference between using observed and predicted satellites in terms of: (left) number of satellites and (right) geometry expressed by PDOP.

Positioning mode	Median Error		RMSE	
	(AT)	(CT)	(AT)	(CT)
RTK	0.057	0.055	0.078	0.106
IMU + odometer within a few seconds	0.151	0.320	0.248	0.205

Table 3.
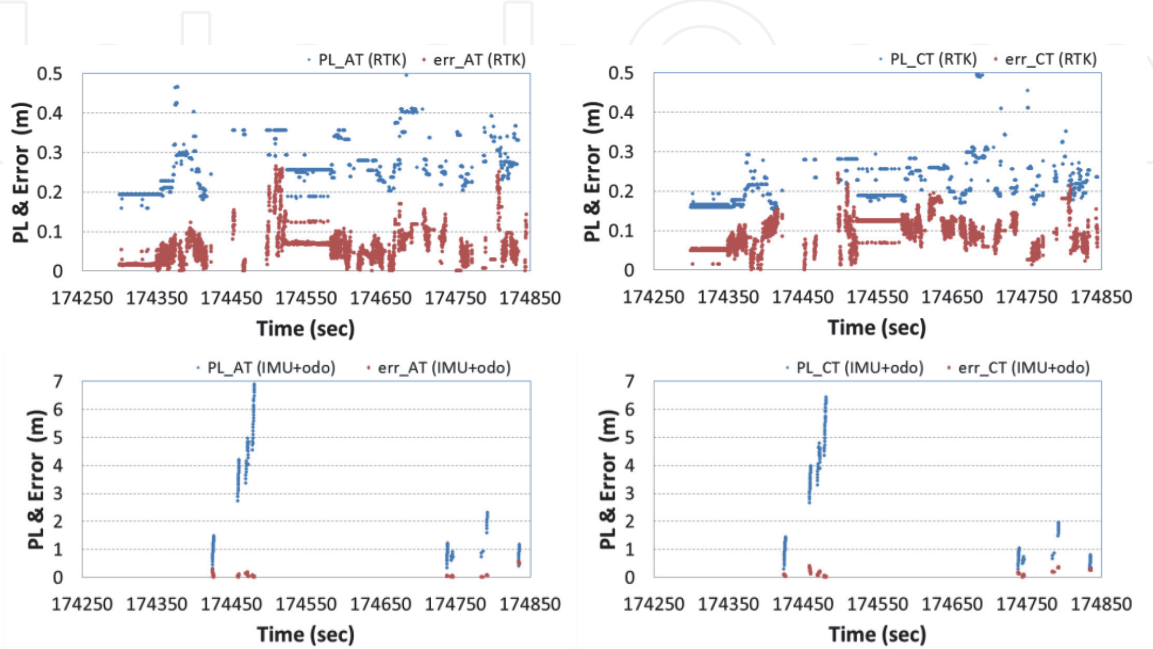*Median positioning error and RMSE for* AT *and* CT *directions (m).*

Figure 8.
PL_AT, PL_CT and PE for the AT (left) and CT (right) for the RTK (top panel), and IMU + odometer positioning (bottom panel), integrity risk = 1×10^{-5}.

calibration. Hence, this method should be limited to bridging RTK positioning only for a few-second period.

Figure 8 shows the time series of the *PL* when the RTK (top panel) and IMU + odometer (bottom panel) were used for the AT and CT directions (shown as *PL_AT* and *PL_CT*) using an integrity risk of 1×10^{-5}. The absolute values of the positioning errors in the *AT* and *CT* directions, i.e. *err_AT* and *err_CT* are depicted in the figure. Note the different scale used. The effectiveness of integrity monitoring algorithm can be assessed by checking that the position errors (*PEs*) are bounded by *PLs*, and availability of integrity monitoring is judged by checking that *PL < AL*. The RTK positioning errors shown in the figure were less than 10 cm and were always bounded by tight protection levels and thus the choice of an alert limit (*AL*) of 1.5 m (e.g. half of a small lane width of 3 m) is sufficient. Likewise, for the majority of IMU + odometer positioning period, the position errors were bounded by the PLs. Thus, positioning integrity was available (i.e. *PL < AL*) for the full period of RTK positioning and during most of IMU + odometer positioning, giving a total availability of integrity monitoring >99.9%.

6. Testing SBAS for ITS

To evaluate the next generation SBAS for ITS applications, Kinematic tests were conducted using two test vehicles in scenarios characterized by different levels of sky-visibility that may be experienced by ITS applications, which included open
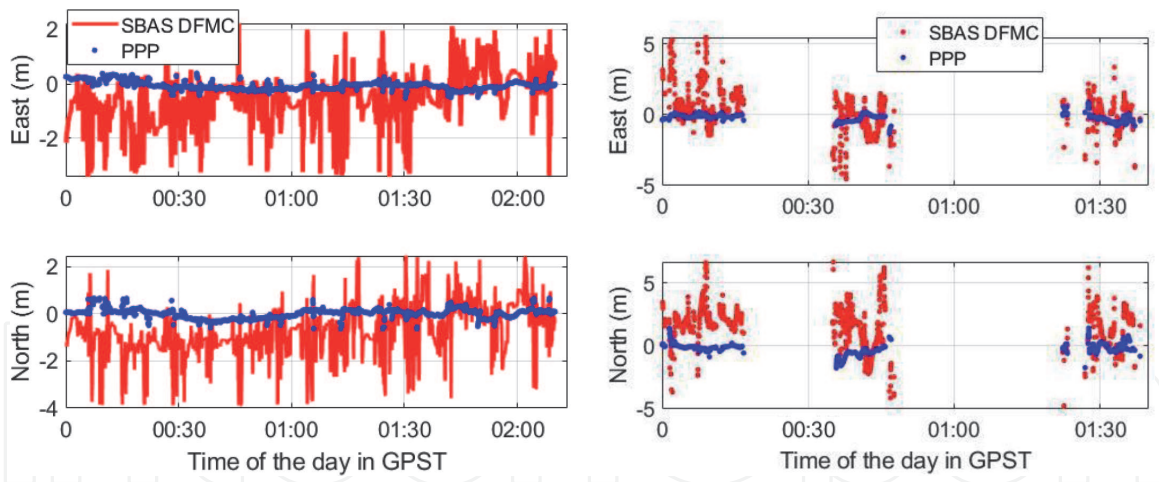
Figure 9.
Results of DFMC SBAS and SBAS-based PPP for open-sky environment (left) and semi-urban environment (right).

sky, semi-urban and urban environments. The tests were carried out in July and August 2018 in Australia. The next-generation SBAS test-bed data was used which provides three types of solutions, L1 SBAS solution, a DFMC SBAS solution using L1/L2 GPS and Galileo E1/E5a measurements, and SBAS-corrections for PPP solution using GPS and Galileo observations (L1/L2 and E1/E5a, respectively). All data were collected and processed at a frequency of 1 Hz. A 'ground truth' for the positions of the vehicle was computed in a post-processing mode through independent relative kinematic positioning - PPK. The same raw code and phase observations used for SBAS-based positioning were used as the rover observations with data from a Continuously Operating Reference Station (CORS), serving as a base station, where the test vehicles were within a radius of eight kilometers from the base station. Only ambiguity-fixed solutions from PPK, with 1–5 cm precision, were used as ground truth.

Figure 9 shows two examples of applying the new generation DFMC and float-ambiguity PPP SBAS in the open-sky (left panel) and semi-urban (right panel) environments. Analysis of results shows that the new SBAS DFMC solutions have slightly better accuracy than the SBAS L1 solutions, but both generate errors between sub-m to more than 2 m. In addition, the multi-constellation PPP solutions have shown to provide the best positioning precision and accuracy among all the tested solution types (L1 SBAS, DFMC SBAS, and SBAS-based PPP) with sub-decimeter level standard deviations after solution convergence [35], provided that enough convergence time is available, which may take up to 30 min. Testing clearly demonstrates that positioning performance of both DFMC SBAS and PPP methods is strongly dependent on the environment of the application, which is linked to the strength of the satellite geometry, number of observed satellites, the presence of multipath and NLOS. When considering the suitability of these findings for ITS applications, results suggest that, in open sky environment, lane identification and collision alert applications can be performed 80% of the time with DFMC SBAS and nearly all the time with PPP. The urban environment was the least promising with low availability for all SBAS solution types.

7. Cooperative positioning tests

A series of experiments with an aim to test the performance of different CP architectures were conducted in the vicinity of Melbourne, Australia. A network of
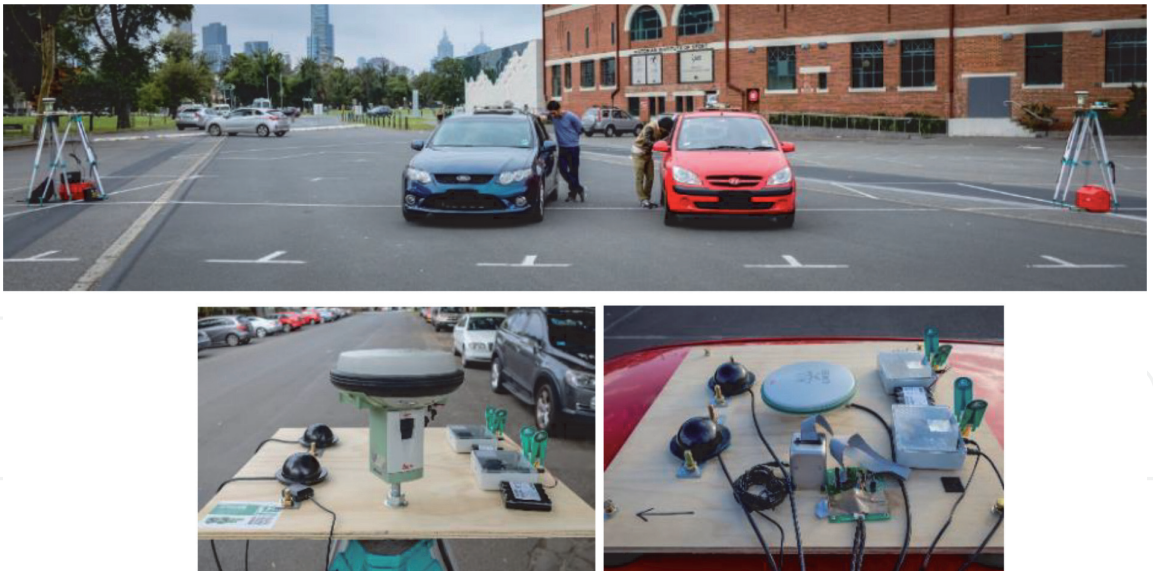
Figure 10.
CP equipment setup—Reference (left) on the car (right).

platforms was employed, with two vehicles acting as moving rovers and two static platforms acting as RSUs, shown in **Figure 10**. The tests were conducted in multiple environment scenarios such as in open sky, residential and dense urban environments. In all, five main sensors were deployed and attached to these platforms, including GNSS, IMU, VSS, UWB and DSRC. The deployment of these sensors on each platform is as described in **Table 4**.

A more suitable architecture for CP in a VANET is one that is decentralized in nature. The proposed architecture is depicted in **Figure 11** (top) where the different color lines represent different input/output similar to the centralized architecture in **Figure 10** (bottom). It can be seen that in this system, each vehicle only uses connections with immediate neighbors, i.e., data does not need to be hoped to a central processor in an event where direct connections between the central processor and vehicles cannot be established. This makes a VANET with a decentralized architecture more efficient in handling scalability compared to a centralized system. However, the nature of a decentralized system disallows for the computation of the network joint posterior, where only marginal posteriors can be calculated. Thus, in terms of the parameter estimation process, it is expected that the decentralized architecture and algorithm would produce less accurate navigation output compared to the centralized architecture. **Figure 11** shows that apart from the absence of a central processor, the decentralized architecture is identical to the centralized one. As before, the local level observations are solved for first, before the resulting information is passed on to the CP processor, utilizing SPAWN or MDSPAWN as

Sensor	Vehicle 1	Vehicle 2	RSU 1	RSU 2
GNSS	Leica GS10	Leica GS10	Leica GS15	Leica GS15
IMU	GX3-45	MMQG	-	-
VSS	Vehicle OBDII	-	-	-
DSRC	MK2	MK2	MK2	MK2
UWB	$1 \times$ P410	$2 \times$ P410	$2 \times$ P410	$2 \times$ P410

Table 4.
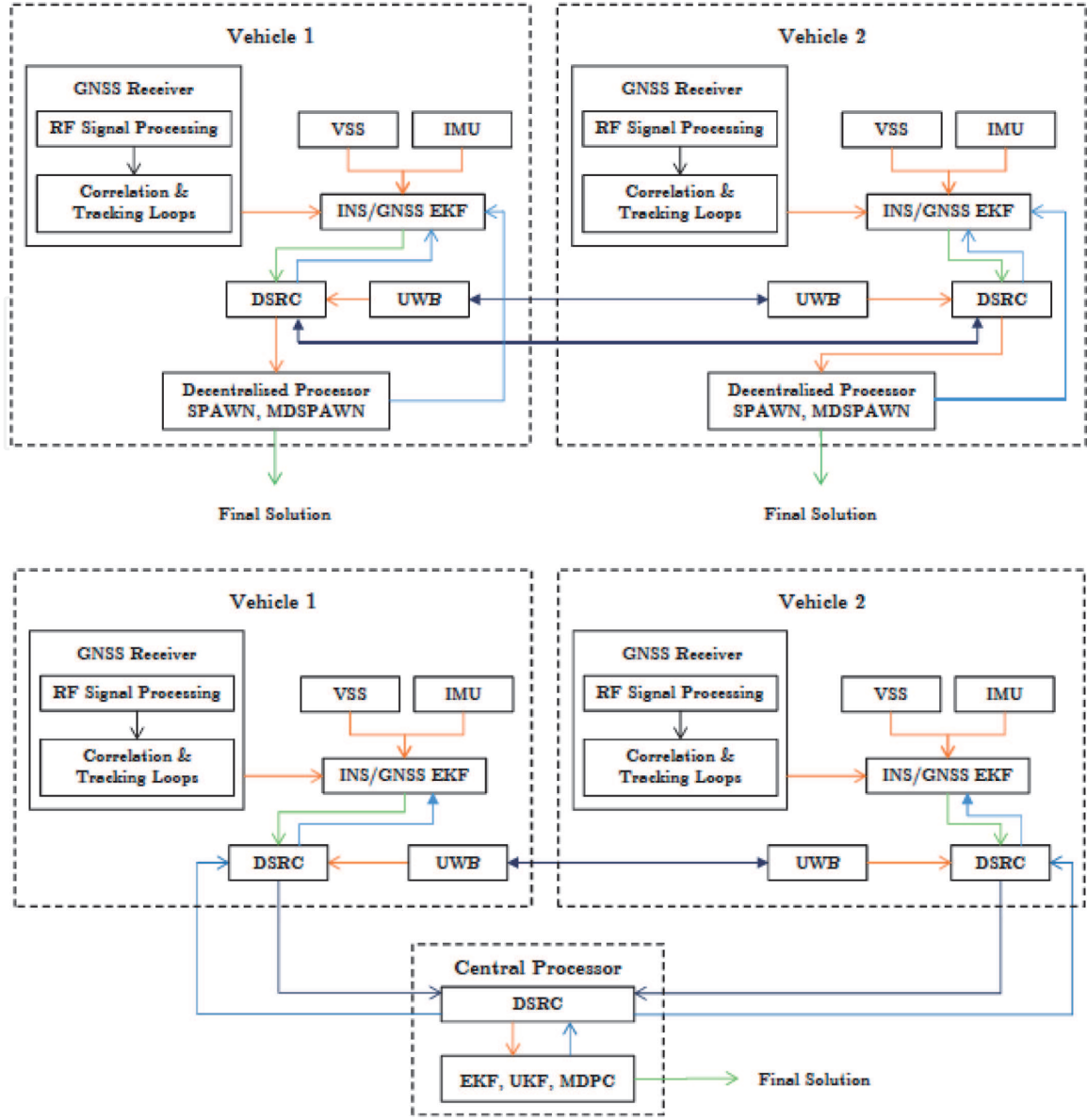*Different Sensor deployment for CP testing.*

Figure 11.
Decentralized CP (top) and centralized CP (bottom), from [40].

the CP state estimator. In this example, the algorithms used for the centralized processing were the standard extended Kalman filter (EKF) [36] and particle filter (PF) [37] as well as an algorithm developed here termed the measurement directed progressive correction (MDPC), which is an improved centralized PF based on [37] for cooperative positioning in difficult environments. The decentralized approaches implemented were the sum product over wireless network (SPAWN) method, which is a fully distributed estimation algorithm, based on a factor graph (FG) and sum product algorithm (SPA) [38, 39]. This was further developed in this research and adopts the measurement directed method on SPAWN, termed the measurement directed SPAWN (MD-SPAWN) algorithm. Full details of these algorithms can be found in [40].

Results obtained from integrating INS, GNSS using real datasets where both non-radio ranging and radio ranging based CP were utilized are summarized in **Table 5**. The table shows that fusing INS and shared raw GNSS observations to form V2V double difference ranging in CP could significantly enhance the positioning accuracies of the participating vehicles in VANET. INS, which provided measurement redundancies and continuous positioning, enables for the CP to continuously operate even when the observed satellites were below the minimum number of

Scenario 2.1	Mean RMSE (m)		Max Error (m)	
	2D	3D	2D	3D
INS/GNSS	2.59	4.77	4.46	10.92
INS/GNSS CP EKF	1.21	2.22	2.45	4.24
INS/GNSS CP MDPC	1.69	3.19	3.20	5.63
INS/GNSS CP SPAWN	1.67	3.24	3.19	4.98
INS/GNSS CP MDSPAWN	1.63	3.09	3.08	4.71

Table 5.
Integrating INS with GNSS in different CP scenarios.

satellites needed in conventional CP system, which is useful in environments that suffer from GNSS signal shadowing. However, this technique is not suitable to be used when the GNSS signals are affected by multipath, which would invariably affect the V2V ranging. When radio ranging was obtained via UWB transceivers, instead of shared raw GNSS observations results obtained were comparable.

8. Conclusion

A proposed system that can be used for ITS is discussed. The system includes low-cost GNSS RTK integrated with MEMS IMU and automotive odometer. This low-cost RTK system can produce an accuracy of less than 0.l m. The Integrity monitoring (IM) approach for this system is presented. The computed PLs were shown to bound the position errors all the time, proven effectiveness of the models. The PLs also suggested that the use of an alert limit of 1.5 m will provide IM availability larger than 99.9%. This can support several ITS applications. A main challenge in positioning using IMU + odometer is that they estimate the time-change in positioning and their biases accumulate with time, the system thus needs frequent resetting. Their bridging of positioning is thus recommended only for a few seconds, where sub-meter accuracy can be obtained.

The next-generation SBAS was also evaluated for ITS applications. It is evident from testing that the positioning performance of both DFMC SBAS and PPP methods is strongly dependent on the environment of application, where SBAS seems only suitable for open sky environment where DFMC SBAS and PPP can provide sub-m/m and dm accuracy, respectively.

To ensure safety, reduce pollution and save energy, reliable positioning with best route selection capability is required for intelligent transport systems. A method for route selection with the capability of predicting precision and integrity of positioning using GNSS integrated with 3D city models is presented. A demonstration of the method was conducted in a semi-urban area in Tokyo. Results show that the 3D city model based algorithm is able to determine LOS satellites with a small margin of error. An improvement can be achieved, for instance, by using higher accuracy 3D models or digital laser scanning 3D models. The method proposed is also suitable to determine locations within the city, where GNSS would not be suitable and other sensors should be used.

Future work includes the use of Lidar sensors and better quality IMUs, and developing new algorithms for the computation of the PLs for these sensors. Additionally, advanced models for weighting GNSS observations under multipath are considered. Finally, more architectures of V2V and VANET are planned.

Acknowledgements

Author details

Ahmed El-Mowafy[1]*, Nobuaki Kubo[2] and Allison Kealy[3]

1 School of Earth and Planetary Sciences, Curtin University, Australia

2 Tokyo University of Marine Science and Technology, Japan

3 School of Science, RMIT University, Australia

*Address all correspondence to: a.el-mowafy@curtin.edu.au

IntechOpen

References

[1] Godha S, Canon ME. GPS/MEMS INS integrated system for navigation in urban areas. GPS Solutions. 2007;**11**(3): 193-203

[2] Yang Y, Mao X, Tain W. A novel method for low-cost IMU aiding GNSS attitude determination. Measurement Science and Technology. 2016;**27**(7): 075003

[3] Yand L, Wu Y, Li Y, Rizos C. An enhanced MEMS-INS/GNSS integrated system with fault detection and exclusion capability for land vehicle navigation in urban areas. GPS Solutions. 2014;**18**(4):593-603

[4] Lu N, Cheng N, Zhang N, Shen X, Mark JW. Connected vehicles: Solutions and challenges. IEEE Internet of Things Journal. 2014;**1**(4):289-299

[5] El-Mowafy A. Pilot evaluation of integrating GLONASS, Galileo and Bei Dou with GPS in ARAIM. Artificial Satellites. 2016;**51**(1):31-44

[6] Blanch J, Walter T, Enge P. Optimal positioning for advanced RAIM. Navigation. 2014;**60**(4):279-289

[7] Rippl M, Martini I, Belabbas B, Michael M. ARAIM operational performance tested. In: Flight Proceedings of ION ITM 2014, San Diego, CA; 27–29 January, 2014. pp. 601-615

[8] El-Mowafy A, Yang C. Limited sensitivity analysis of ARAIM availability for LPV-200 over Australia. Advances in Space Research. 2016;**57**(2): 659-670

[9] Khanafesh S, Pervan P. New approach for calculating position domain integrity risk for cycle resolution in carrier phase navigation systems. IEEE Transactions on Aerospace and Electronic Systems. 2010;**46**(1):296-306

[10] Cezón A, Cueto M, Fernández I. Analysis of multi-GNSS service performance assessment: ARAIM vs. IBPL performances. In: Proceedings of the ION GNSS 2013, Nashville; 16–20 September, 2013. pp. 2654-2663

[11] Wang K, El-Mowafy A. Integrity monitoring of intelligent transport system using Kalman filter based RTK. Journal of Geodesy. 2019. In Press

[12] Margaria D, Falletti E. A novel local integrity concept for GNSS receivers in urban vehicular contexts. In: Proceedings of the IEEE/ION PLANS 2014, Monterey, CA, USA; 5–8 May, 2014. pp. 413-425

[13] Santa J, Ubeda B, Toledo R, Skarmeta AFG. Monitoring the position integrity in road transport localization based services. In: IEEE Vehicular Technology Conference, Montreal, Quebec; 2006. pp. 1-5

[14] Zhu N, Betaille D, Marais J, Berbineau M. GNSS position integrity in urban environments: A review of literature. IEEE Transactions on Intelligent Transportation Systems. 2018;**19**(9):2762-2778

[15] Imparato D, El-Mowafy A, Rizos C, Wang J. A review of SBAS and RTK vulnerabilities in intelligent transport systems applications. In: Proceedings of the IGNSS Symposium 2018, Sydney; 7–9 February, 2018. pp. 1-18

[16] Hsu L, Gu Y, Kamijo. SNLOS correction/exclusion for GNSS measurement using RAIM and city building models. Sensors. 2015;**15**: 17329-17349

[17] El-Mowafy A, Kubo N. Integrity assessment of vehicle positioning for journey planning in urban environment using RTK and 3D city models. Journal of Navigation. 2019. In Press

[18] El-Mowafy A. Chapter 7: Precise real-time positioning using network RTK. In: Global Navigation Satellite Systems: Signal, Theory and Applications. Rijeka, Croatia: InTech Publisher; 2012. pp. 161-188

[19] El-Mowafy A, Wang K. Second generation SBAS performance analysis and bridging positioning and integrity monitoring during SBAS outages. In: Proceedings of the ION GNSS+ 2019, Miami, FL; 16–20 September, 2019. pp. 2842-2854

[20] Misra P, Enge P. Global Position System: Signals, Measurements, and Performance. Lincoln, Massachusetts: Ganga-Jamuna Press; 2006

[21] Zumberge JF, Heflin MB, Jefferson DC, Watkins MM, Webb FH. Precise point positioning for the efficient and robust analysis of GPS data from large networks. Journal of Geophysical Research. 1997;**102**(B3): 5005-5017

[22] Kouba J. A Guide to Using International GNSS Service (IGS) Products. 2015. Available from: https://kb.igs.org/hc/en-us/articles/201271873-A-Guide-to-Using-the-IGS-Products [Accessed: June 2019]

[23] Mahmoud A, Noureldin A, Hassanein H. Integrated positioning for connected vehicle. IEEE Transactions on Intelligent Transportation Systems. 2019. DOI: 10.1109/TITS.2019.2894522

[24] El-Sheimy N, Hou H, Niu X. Analysis and modeling of inertial sensors using AV. IEEE Transactions on Instrumentation and Measurement. 2008;**57**(1):140-149

[25] El-Mowafy A, Kubo N. Integrity monitoring of vehicle positioning in urban environment using RTK-GNSS, IMU and speedometer. Measurement Science and Technology. 2017;**28**(5): 055102

[26] Austroads. Cooperative ITS Strategic Plan. Austroads Research Report AP-R413-12. Austroads: Sydney; 2012

[27] Noah J, Smith B, Park B. Traffic signal control with connected vehicles. Transportation Research Record: Journal of the Transportation Research Board. 2013;**2381**(1):65-72

[28] Richter E, Obst M, Schubert R, Wanielik G. Cooperative relative localization using vehicle-to-vehicle communications. In: Proceedings of the 12th International Conference on Information Fusion, Seattle, WA, USA; July 2009. pp. 126-131

[29] Möller T, Trumbore B. Fast, minimum storage ray-triangle intersection. Journal of Graphics Tools. 1997;**2**(1):21-28

[30] El-Mowafy A, Kubo N. Integrity monitoring for positioning of intelligent transport systems using integrated RTK-GNSS, IMU and vehicle odometer. IET Intelligent Transport Systems. 2018; **12**(8):901-908

[31] Rife J, Pullen S, Enge P, Pervan B. Paired overbounding for nonideal LAAS and WAAS error distributions. IEEE Transactions on Aerospace and Electronic Systems. 2006;**42**(4): 1386-1395

[32] Chalko TJ. Estimating accuracy of GPS Doppler speed measurement using speed dilution of precision parameter. NU Journal of Discovery. 2009;**6**:4-9

[33] Zhao Y. GPS/IMU integrated system for land vehicle navigation based on MEMS [Thesis]. Stockholm, Sweden: KTH Royal Institute of Technology; 2011

[34] Meguro J, Kojima Y, Suzuki N, Teramoto E. Positioning technique based on vehicle trajectory using GPS

raw data and low-cost IMU.
International Journal of Automotive
Engineering. 2012;**3**(2):75-80

[35] El-Mowafy A, Cheung N,
Rubinov E. Performance analysis of
using the next generation Australian
SBAS with precise point positioning
capability for ITS. In: Proceedings of the
ENC2019, Warsaw, Poland; 9–12 April,
2019. pp. 1-8

[36] Welch G, Bishop G. An Introduction
to Kalman Filter. Chapel Hill:
Department of Computer Science,
University of North Carolina; 2006

[37] Morelande M, Moran B, Brazil M.
Bayesian node localisation in wireless
sensor networks. In: IEEE International
Conference on A, S and S Processing,
2008 (ICASSP 2008); March 2008.
pp. 2545-2548

[38] Caceres M, Penna F, Wymeersch H,
Garello R. Hybrid cooperative
positioning based on distributed belief
propagation. Selected areas in
communications. IEEE Journal. 2011;
29(10):1948-1958

[39] Wymeersch H, Lien J, Win M.
Cooperative localization in wireless
networks. Proceedings of the IEEE.
2009;**97**(2):427-450

[40] Rabiain AH. Robust cooperative
positioning for VANETs based on multi
sensor system & enhanced estimation
algorithms [PhD dissertation].
Melbourne, Australia: University of
Melbourne; 2018